View metadata, citation and similar papers at core.ac.uk

brought to you by CORE

provided by Hal-Diderot

Steady and fluctuating inner core rotation in numerical geodynamo models

Julien Aubert, Mathieu Dumberry

To cite this version:

Julien Aubert, Mathieu Dumberry. Steady and fluctuating inner core rotation in numerical geodynamo models. Geophysical Journal International, Oxford University Press (OUP), 2010, 184 (1), pp.162-170. <10.1111/j.1365-246X.2010.04842.x>. <insu-01308309>

HAL Id: insu-01308309

https://hal-insu.archives-ouvertes.fr/insu-01308309

Submitted on 27 Apr 2016

HAL is a multi-disciplinary open access archive for the deposit and dissemination of scientific research documents, whether they are published or not. The documents may come from teaching and research institutions in France or abroad, or from public or private research centers.

L'archive ouverte pluridisciplinaire **HAL**, est destinée au dépôt et à la diffusion de documents scientifiques de niveau recherche, publiés ou non, émanant des établissements d'enseignement et de recherche français ou étrangers, des laboratoires publics ou privés.

Geophysical Journal International

Geophys. J. Int. (2011) **184,** 162–170 doi: 10.1111/j.1365-246X.2010.04842.x

Steady and fluctuating inner core rotation in numerical geodynamo models

Julien Aubert[1] and Mathieu Dumberry[2]

[1]*Dynamique des Fluides Géologiques, Institut de Physique du Globe de Paris, Université Paris-Diderot, INSU/CNRS,* 1*, rue Jussieu,* 75238, *Paris Cedex* 05, *France. E-mail: aubert@ipgp.fr*
[2]*Department of Physics, University of Alberta, Edmonton, AB,* T6G 2G7, *Canada*

Accepted 2010 October 5. Received 2010 September 6; in original form 2010 June 4

SUMMARY

We present a systematic survey of numerical geodynamo simulations where the inner core is allowed to differentially rotate in the longitudinal direction with respect to the mantle. We focus on the long-term behaviour of inner core rotation, on timescales much longer than the overturn time of the fluid outer core, including the steady component of rotation. The inner core is subject to viscous and magnetic torques exerted by the fluid outer core, and a gravitational restoring torque exerted by the mantle. We show that the rate of steady inner core rotation is limited by the differential rotation between spherical surfaces that the convective dynamics can sustain across the fluid outer core. We further show that this differential rotation is determined by a torque balance between the resistive Lorentz force and the Coriolis force on spherical surfaces within the fluid core. We derive a scaling law on the basis of this equilibrium suggesting that the ratio of the steady inner core rotation to typical angular velocity within the fluid core should be proportional to the square root of the Ekman number, in agreement with our numerical results. The addition of gravitational coupling does not alter this scaling, though it further reduces the amplitude of inner core rotation. In contrast, the long-term fluctuations in inner core rotation remain proportional to the fluid core angular velocity, with no apparent dependency on the Ekman number. If the same torque balance pertains to the Earth's core conditions, the inner core rotation then consists in a very slow super rotation of a few degrees per million years, superimposed over large fluctuations (at about a tenth of a degree per year). This suggests that the present-day seismically inferred inner core rotation is a fragment of a time-varying signal, rather than a steady super rotation. For the inner core rotation fluctuations not to cause excessive variations in the length-of-day, the strength of the gravitational coupling between the inner core and the mantle must be smaller than previously published values. We finally explore how the torque balance which we observe in our models could be altered in planetary cores, yielding possibly larger values of the steady rotation.

Key words: Earth rotation variations; Dynamo: theories and simulations.

1 INTRODUCTION

The Earth's fluid outer core separates the solid, electrically conducting inner core from the mantle, and is subject to vigorous thermo-chemical convection, which produces the main magnetic field of the planet through the geodynamo process. Geodynamical arguments suggest that the inner core is very probably subject to a differential longitudinal rotation with respect to the mantle (Gubbins 1981): electromagnetic torques with a nominal strength of 10^{19} N m are sufficient to accelerate the inner core to velocities of about a tenth of a degree per year within only a few days. Early numerical models producing self-consistent dynamos (Glatzmaier & Roberts 1996) have indeed shown that these torques entrain the inner core into long-term corotation with the overlying fluid, yielding typical inner core differential rotation rates of about a degree per year in the steady state. These findings motivated the seismological search for inner core rotation. Positive reports were initially given by Song & Richards (1996), who detected systematic variations of differential traveltimes between the PKP(DF) phase refracted in the inner core and the PKP(BC) phase turning in the bottom outer core for three different paths, which they attributed to the rotation of a tilted inner core anisotropy axis. The topic is however still controversial (see Souriau 2007, for a review), as other seismic ray paths, or even other methods based for instance on normal mode analysis (Laske & Masters 2003) did not yield the same conclusion. More recently, analyses of the PKiKP phase which is reflected off the inner core boundary (Wen 2006; Cao *et al.* 2007) have revealed temporal changes in the inner core boundary topography sampled by

Downloaded from http://gji.oxfordjournals.org/ at INIST-CNRS on April 27, 2016

© 2010 The Authors
Geophysical Journal International © 2010 RAS

earthquake doublets. This can again be attributed to inner core differential rotation, but other explanations exist, such as rapid changes in topography of a fixed inner core. Another recently highlighted complication is that if inner-core differential rotation exists, its rate appears to also have changed over the last decades (Song & Poupinet 2007), in apparent conflict with early numerical simulation results where the steady part of inner core rotation was dominating the temporal fluctuations.

The hypothesis of a steady inner core rotation is also problematic if the gravitational coupling between density anomalies in the lower mantle and the corresponding topography anomalies on the inner core surface is considered. A rotating inner core would carry its surface topography out of a longitudinal alignment with density anomalies in the mantle, resulting in a strong restoring gravitational torque (Buffett 1996). Corotation between the inner core and its overlying fluid is thus likely to be broken. With gravitational coupling present, a steady inner core rotation remains possible, albeit at a slower rate than the overlying fluid and only if the inner core topography can deform viscously to adjust to the imposed gravitational potential from the mantle (Buffett 1997). Numerical geodynamo simulations including these concepts have shown that the steady inner core rotation can be efficiently inhibited by gravitational coupling, while short timescale fluctuations dominate (Buffett & Glatzmaier 2000). The scenario of an inner core undergoing a fluctuating differential rotation is however also problematic: by virtue of gravitational coupling, inner core rotation variations should entrain variations in mantle rotation and hence, variations in the length of day (Buffett 1996). If the seismically inferred inner core rotation rate indeed represents an irregular rotation, it has been shown that the amplitude of the length-of-day changes induced by this process might actually exceed the observed variations (Buffett & Creager 1999; Dumberry 2007).

The purpose of this study is to expose the fundamental mechanisms constraining the amplitude of long-term inner core rotation in numerical geodynamo models, and to extend earlier studies (Glatzmaier & Roberts 1996; Aurnou *et al.* 1998; Hollerbach 1998; Buffett & Glatzmaier 2000) by taking advantage of the recent increase in computer power, which allows systematic analysis of the parameter space and derivation of scaling laws. In Section 2 we present the numerical model and numerical data set. In Section 3 we present the scaling laws which have been obtained and corresponding theoretical models. The results are subsequently discussed in Section 4.

2 NUMERICAL MODEL

2.1 Model description

We consider a convecting, electrically conducting, incompressible fluid of density ρ, viscosity ν and electrical conductivity σ in a spherical shell between radii r_i and $r_o (D = r_o - r_i$ is the shell gap) in a spherical coordinate frame (r, θ, φ). The aspect ratio is $r_i/r_o = 0.35$, as in the Earth's core. The shell is rotating about an axis $\mathbf{e}_z$ with constant angular velocity Ω. Thermal convection is modelled in the Boussinesq approximation, and electromagnetic induction in the magnetohydrodynamic approximation. Our numerical simulations are fairly standard (see Christensen & Aubert 2006, for a complete description and details on the equations), except for the implementation of inner core rotation dynamics, which is detailed in Section 2.2.

One of the fundamental differences of our approach with respect to previous studies is the treatment of the viscosity in the numerical model. Viscosity is usually the least realistic variable of numerical dynamos, because of the computational cost involved in resolving the enormous disparity between viscous and magnetic diffusivities. For that reason, various approximations have been employed (e.g. Glatzmaier & Roberts 1996; Buffett & Glatzmaier 2000), including viscous hyperdiffusivity and the implementation of free-slip mechanical boundary conditions at the inner core boundary. In contrast, we use non-slip boundary conditions between the inner and outer core, and we do not resort to viscous hyperdiffusivity in the fluid outer core. We then assess the effects of viscosity by performing simulations at varying values of the Ekman number $E = \nu/\Omega D^2$, where ν is the fluid outer core viscosity, and obtaining scaling laws for the phenomena which are controlled by the residual (and too high) viscosity employed in our models. This approach yields a theoretical formulation which is greatly simplified and easy to benchmark with other computer codes (Christensen *et al.* 2001).

The second main difference in our approach concerns the method by which we analyse the rate of inner core rotation. Since in the absence of gravitational coupling the inner core should be corotating with the fluid directly above the inner core boundary, the differential rotation of the inner core with respect to the mantle must then be equivalent to the amount of differential rotation between spherical surfaces that can be sustained across the fluid outer core by convective dynamics. This forms the basis of our scaling law and this is why it is important to maintain complete consistency between the physical properties entering the dynamics of the inner core, and those describing the outer core flow, a principle which guides our choice of boundary conditions at the inner boundary. The velocity field also obeys rigid boundary conditions at the external boundary of the model, and fixed temperature boundary conditions are adopted. The magnetic field obeys insulating boundary conditions at the external boundary. At the internal boundary, the field is matched to that in a conducting solid medium of same conductivity and density as that of the fluid.

Table 1 summarizes the 19 runs performed for this study and their relevant input parameters and outputs. The equations and definitions for the Rayleigh number Ra^*, Ekman number E, Prandtl and magnetic Prandtl numbers Pr and Pm, and for the assumed azimuthal symmetry m_c can be found in Christensen & Aubert (2006). We explore a computationally intensive parameter regime where viscous torques in the fluid shell are much smaller than magnetic torques (see Fig. 3). In the Earth's core, we expect nominal viscous torques amounting to 10^{12}–10^{15} N m (Aurnou & Olson 2000) , illustrating that this regime is geophysically relevant. The main output parameters of our study are the inner core steady rotation rate $\Omega_{\rm ic}$, and the standard deviation of its temporal fluctuations $\Delta\Omega_{\rm ic}$. Additionally, the magnitude of the steady outer core zonal flow is measured by taking the time-averaged, root-mean-squared value u_φ of the azimuthal flow field in the whole shell. A magnetic field amplitude B_r(ic) at the inner boundary is retrieved from the time-averaged energy of the poloidal magnetic field threading the inner core.

The models are integrated using the PARODY code (see Aubert *et al.* 2008, for details), which uses finite differences in the radial direction with up to 240 gridpoints, and a spherical harmonic decomposition in the lateral direction up to degree and order 320. The code uses distributed-memory parallelism among up to 60 processors. Owing to the computational challenges of the parameter space studied, the real time duration of each run is on the order of 1 week to 1 month. All models produce a dipole-dominated magnetic field which does not reverse. Time averages are typically taken over a large number of core overturn times D/U, where U is a typical convective velocity in the outer core.

Downloaded from http://gji.oxfordjournals.org/ at INIST-CNRS on April 27, 2016

Table 1. Description of input parameters and outputs for the 19 models presented in this study (see text for definitions of the various quantities). The Prandtl number is set to 1 for all simulations.

E	Ra^*	$\frac{Ra^*}{Ra_c^*}$	Pm	m_c	$\frac{\Gamma\tau}{\rho\nu D^3}$	$\frac{\Omega_{ic}}{\nu/D^2}$	$\frac{\Delta\Omega_{ic}}{\nu/D^2}$	$\frac{u_\varphi}{\nu/D}$	$\frac{\sigma B_r(ic)^2}{\rho\Omega}$
$3\cdot10^{-5}$	0.036	14.1	2	1	0	99.3	43.9	32.2	3.6
$3\cdot10^{-5}$	0.036	14.1	0.5	1	0	131.2	22.6	33.4	1.9
$3\cdot10^{-5}$	0.054	21.1	0.5	1	0	215.6	42.9	57.8	2.1
$3\cdot10^{-5}$	0.072	28.2	0.5	1	0	333.8	64.3	81.0	1.8
$3\cdot10^{-5}$	0.072	28.2	0.5	1	50	254.3	43.7	80.2	1.9
$3\cdot10^{-5}$	0.072	28.2	0.5	1	500	82.0	16.8	73.6	1.5
$3\cdot10^{-5}$	0.072	28.2	0.5	1	5000	11.0	2.47	71.2	1.3
$3\cdot10^{-5}$	0.072	28.2	0.5	1	50000	1.2	0.27	71.9	1.1
10^{-5}	0.02	19.0	0.5	2	0	209.0	83.21	97.7	1.5
10^{-5}	0.03	28.5	0.5	2	0	290.0	126.6	147.8	1.6
10^{-5}	0.04	38.1	0.5	2	0	446.1	172.1	178.0	1.7
10^{-5}	0.04	38.1	0.15	2	0	248.6	111.0	130.3	1.7
$3\cdot10^{-6}$	0.0162	39.1	0.5	4	0	559.7	265.3	290.8	1.4
$3\cdot10^{-6}$	0.0162	39.1	0.1	4	0	310.3	199.0	235.3	1.0
$3\cdot10^{-6}$	0.0162	39.1	0.1	4	50	315.4	207.3	238.4	1.0
$3\cdot10^{-6}$	0.0162	39.1	0.1	4	500	276.9	107.2	218.9	1.1
$3\cdot10^{-6}$	0.0162	39.1	0.1	4	5000	89.0	26.9	249.2	1.2
$3\cdot10^{-6}$	0.0162	39.1	0.1	4	50000	10.9	3.0	258.9	1.1
$3\cdot10^{-6}$	0.0162	39.1	0.075	4	0	381.3	227.4	244.2	0.7

2.2 Torque balance at the inner core boundary and inner core rotation

The inner core is modelled as a full solid sphere of radius r_i, with homogeneous density ρ and electrical conductivity σ both equal to the values they have in the fluid. It is allowed to rotate in the longitudinal direction with angular velocity ω_{ic} with respect to the outer boundary (the mantle), which is assumed not to depart from the background planetary rotation rate Ω. The latter approximation is justified by the fact that the mantle has a much larger moment of inertia than the core. The expected variations of mantle angular velocity are therefore minute with respect to the long-term components of inner core rotation. Additionally, the inner core is assumed to have a finite viscous relaxation time τ (Buffett 1997). The conservation of inner core angular momentum is expressed as

$$\frac{8}{15}\rho\pi r_i^5\frac{\mathrm{d}\omega_{ic}}{\mathrm{d}t} = \underbrace{\rho\nu\int_{ICB} s^2\frac{\partial \mathrm{u}_\varphi/\mathrm{s}}{\partial r}\mathrm{d}S}_{\text{viscous torque}} + \underbrace{\frac{r_i}{\mu_0}\int_{ICB}\mathrm{B_r B}_\varphi\sin\theta\,\mathrm{d}S}_{\text{magnetic torque}} - \underbrace{\Gamma\tau\,\omega_{ic}}_{\text{gravitational torque}}, \quad (1)$$

where ν is the fluid viscosity, s the cylindrical radius, u_φ the axisymmetric azimuthal velocity field, μ_0 the magnetic permeability, $\mathrm{B_r}$ and B_φ the radial and azimuthal magnetic field components, ICB denotes the surface of the inner boundary and Γ the amplitude constant for gravitational coupling to the outer boundary.

Our implementation of gravitational coupling is similar to that performed in previous works (Buffett 1997; Buffett & Glatzmaier 2000; Mound & Buffett 2006; Dumberry 2007). We assume that a misalignment angle Φ between the inner core and mantle causes a restoring torque $\Gamma_G = -\Gamma\Phi$ on the inner core, where Γ is the gravitational coupling constant. The misalignment angle obeys

$$\frac{\mathrm{d}\Phi}{\mathrm{d}t} = \omega_{ic} - \frac{\Phi}{\tau}. \quad (2)$$

Our numerical models are intended to describe the long-term behaviour of inner core rotation, which comprises its steady part and fluctuations on timescales longer or equal to the overturn time, which is about 100 yr in the Earth's core (Aubert *et al.* 2007). Indeed, due to their large viscosity, numerical dynamos usually fail at describing the system fluctuations on timescales much smaller than the overturn time. For fluctuations at a longer timescale than the viscous relaxation time τ of the inner core, we expect $\mathrm{d}\Phi/\mathrm{d}t \ll \Phi/\tau$. Assuming that τ is shorter than 100 yr, a reasonable assumption, our simulations are in the long-term range where eq. (2) can be approximated by $\Phi = \tau\omega_{ic}$. The gravitational torque thus writes $\Gamma_G = -\Gamma\tau\omega_{ic}$, in accordance with our implementation in eq. (1).

3 RESULTS

3.1 Steady inner core rotation without gravitational coupling

We start our analysis by studying (Fig. 1) the steady component of inner core rotation, in a reference situation where gravitational coupling is absent ($\Gamma\tau = 0$). The steady outer core fluid flow is a baroclinic thermal wind (Aurnou *et al.* 1996; Aubert 2005), preferentially flowing eastwards near the inner core (Glatzmaier & Roberts 1996). The inner core is corotating with the immediately overlying outer core fluid, a trivial consequence of our choice of mechanical boundary conditions. This naturally leads to consider a component of the thermal wind flow, the solid-body rotation rate of a spherical surface $S(r)$ at radius r.

$$\Omega_f(r) = \frac{3}{8\pi r^4}\int_{S(r)}\gamma(r,\theta)\,\mathrm{d}S, \quad (3)$$

where $\gamma(r,\theta) = r\cdot\sin\theta\cdot\langle\mathrm{u}_\varphi\rangle(r,\theta)$ is the azimuthally and time-averaged angular momentum density (as represented in Figs 1a–c). The solid-body rotation is not a dominant part of the thermal wind flow, but its rate at the inner core boundary matches the inner core rotation rate (Fig. 1d), while all other outer core flow components vanish at that boundary. Fig. 1(d) additionally shows that the profile of $\Omega_f(r)$ undergoes little change when control parameters are varied, and is bound by the inner core rotation rate Ω_{ic}. In what follows, we will thus only use the parameter Ω_{ic} to evaluate the order of

Downloaded from http://gji.oxfordjournals.org/ at INIST-CNRS on April 27, 2016

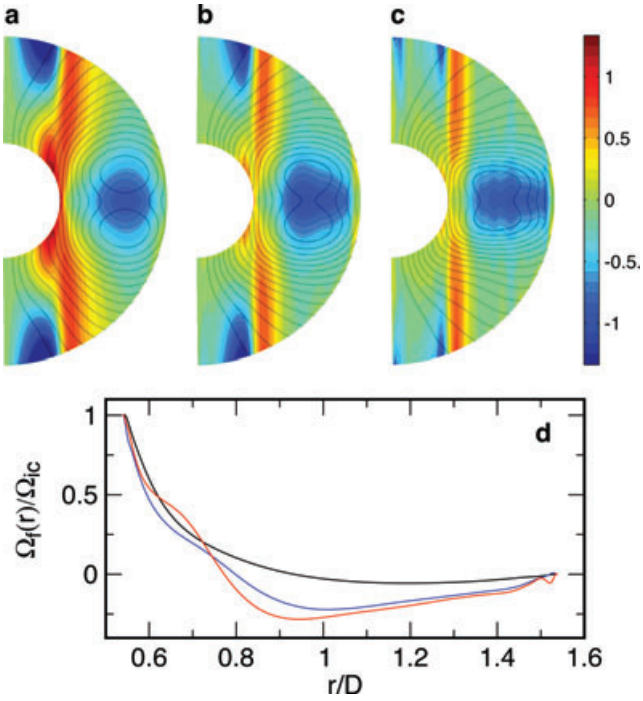

Figure 1. (a), (b) and (c) Meridional plane projections (colours, red is eastwards) of the azimuthally and time-averaged angular momentum density $\gamma = r \cdot \sin\theta \cdot \langle u_\varphi \rangle(r,\theta)$, where $\langle u_\varphi \rangle$ is the time-averaged zonal flow field. Amplitudes are normalized by Du_φ, where u_φ is the root-mean-squared, time-averaged value of the zonal flow field within the fluid shell. Axisymmetric poloidal lines of the dynamo-generated magnetic field are overplotted (grey lines). Dimensionless parameters for the three models presented are, as defined in ref. Christensen & Aubert (2006): (a) $E = 3 \cdot 10^{-5}$, $Ra^* = 0.072$, $Pm = 0.5$; (b) $E = 10^{-5}$, $Ra^* = 0.04$, $Pm = 0.15$; (c) $E = 3 \cdot 10^{-6}$, $Ra^* = 0.0162$, $Pm = 0.1$. All models have $Pr = 1$ and $\Gamma\tau = 0$. (d) Radial profile of the time-averaged solid body rotation rate $\Omega_f(r) = \int 3\gamma/8\pi r^4 \, dS$ of a fluid sphere, normalized by the inner core rotation rate $\Omega_{ic} = \Omega_f(r_i)$. The three lines correspond to the cases presented in panels (a) black, (b) blue and (c) red.

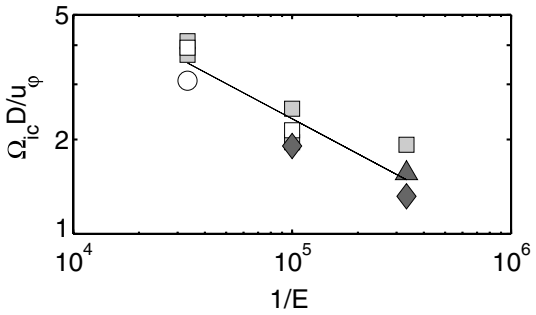

Figure 2. Ratio $\Omega_{ic} D/u_\varphi$ of the steady inner core rotation to fluid outer core angular velocity, as a function of the inverse Ekman number $1/E$. Symbols fill colour denotes the level of departure of the Rayleigh number Ra^* from the critical Rayleigh number Ra_c^*: white for $10 \leq Ra^*/Ra_c^* < 20$, grey for $20 \leq Ra^*/Ra_c^* < 30$ and dark grey for $Ra^*/Ra_c^* > 30$. Symbol shape denotes the value of the magnetic Prandtl number Pm: triangles for $Pm < 0.1$, diamonds for $0.1 \leq Pm < 0.5$, squares for $0.5 \leq Pm < 1$ and circles for $Pm \geq 1$. The solid line is the result of a least-squares logarithmic fit yielding $\Omega_{ic} D/u_\varphi = 235E^{0.4}$. The 2σ uncertainty range on exponent is ± 0.1.

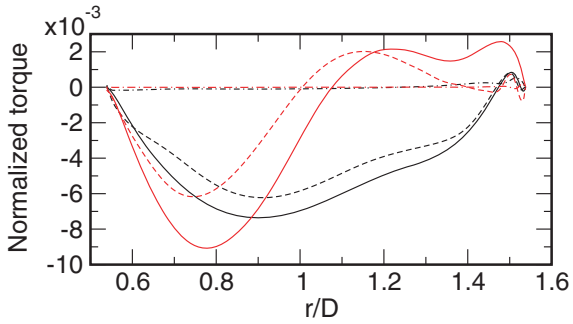

Figure 3. Radial profile of the spherical and time average of the magnetic torque Γ_M (solid line), opposite of the Coriolis torque $-\Gamma_C$ (dashed line) and viscous torque (dot-dash line), for the models presented in Fig. 1(a) black and (c) red. The radius r is normalized by the shell gap D. Torques are normalized by $\rho\Omega\Omega_{ic} D^5$, such that the normalized amplitude of the magnetic torque is equal to the Elsasser number $\Lambda = K\sigma B_r^2/\rho\Omega$ measuring the interaction between poloidal magnetic field and differential rotation. The residual imbalance between the torques is due to a torque Γ_R associated with Reynolds stresses in the fluid (see main text for the definitions of the torques).

magnitude of the solid-body rotation of fluid spheres with respect to the mantle (and its gradients).

Figs 1(a)–(c) illustrate a key phenomenon: as the Ekman number is decreased, the thermal wind immediately overlying the inner core becomes increasingly confined to the surface of the axial cylinder tangent to the inner core (tangent cylinder). The solid-body rotation part of the thermal wind close to the inner boundary—the part connected to the inner core rotation rate—becomes then proportionally smaller with respect to the rest of the outer core flow. This effect is quantified on Fig. 2, where we find that the ratio of the steady inner core rotation rate Ω_{ic} to the typical outer core angular velocity u_φ/D scales as $E^{0.4}$. As we demonstrate later, the fundamental reason for this phenomenon is reminiscent of Ferraro's law of corotation (Ferraro 1937): at low E, the dominantly dipolar magnetic field threading the outer core prohibits large gradients of the fluid spheres solid-body rotation $\Omega_f(r)$, and hence large values of Ω_{ic}.

Our goal is to formulate a scaling law for the inner core rotation rate. The time average of the torque balance (1) at the inner core boundary is a natural starting point, but we note that it is impractical for several reasons. First, it does not explicitly involve the inner core rotation rate, but rotation rate gradients (in the case of the viscous torque). Second, a closer inspection of the inner boundary in the simulations without gravitational coupling reveals that long-term corotation is almost perfectly enforced within the viscous boundary layer. This results in a vanishing time-averaged viscous torque at the inner boundary and a correspondingly vanishing magnetic torque (see Fig. 3), thus rendering the evaluation of the balance rather delicate. Third, the torque balance at the inner core boundary is sensitive on the choice of boundary conditions and torques applied at the boundary (especially gravitational coupling). Keeping in mind that the steady inner core rotation rate is ultimately bound by that of the overlying fluid, we turn to a more general framework, where we evaluate a torque balance for a spherical surface $S(r)$ with an external radius r located within the fluid shell ($r_i < r < r_e$), enclosing a volume $V(r)$. It should be noted that the balance which we are about to derive could be evaluated on other control surfaces and volumes, or even pointwise. However, only the choice of spheres as control surfaces reveals the dependency of the resulting magnetic torque on the solid-body rotation of these spherical surfaces, and hence on the inner core rotation. The axial torque balance derived from the Navier–Stokes equation presented in Christensen & Aubert (2006)

Downloaded from http://gji.oxfordjournals.org/ at INIST-CNRS on April 27, 2016

writes

$$\frac{\mathrm{d}L}{\mathrm{d}t} = \underbrace{\rho \int_{V(r)} [-\mathbf{r} \times (\mathbf{u} \cdot \nabla)\mathbf{u}] \cdot \mathbf{e}_z \, \mathrm{d}V}_{\text{Reynolds stress torque } \Gamma_R} + \underbrace{2\rho\Omega \int_{V(r)} -\mathbf{r} \times (\mathbf{e}_z \times \mathbf{u}) \cdot \mathbf{e}_z \, \mathrm{d}V}_{\text{Coriolis torque } \Gamma_C} + \underbrace{\rho\nu \int_{S(r)} s^2 \frac{\partial \mathrm{u}_\varphi / \mathrm{s}}{\partial r} \mathrm{d}S}_{\text{viscous torque } \Gamma_\nu} + \underbrace{\frac{r}{\mu_0} \int_{S(r)} \mathrm{B_r B}_\varphi \sin\theta \, \mathrm{d}S}_{\text{magnetic torque } \Gamma_M}. \quad (4)$$

Here L is the angular momentum of our control volume $V(r)$, and $\mathbf{u}$ is the velocity field. The buoyancy force, which is parallel to the radius vector $\mathbf{r}$, and the pressure gradient, which is univariate, do not contribute to the above balance. At steady state, we have $\mathrm{d}L/\mathrm{d}t = 0$ and the sum of the torques should vanish. The time-averaged viscous, Coriolis and magnetic torques Γ_ν, Γ_C and Γ_M are computed for two models in Fig. 3. For both models, the viscous torque is negligible outside the thin viscous boundary layer adjacent to the outer boundary (the viscous torque vanishes at the corotating internal boundary). Indeed a quasi-Taylor state is reached at $E = 3{\cdot}10^{-5}$ and below (Takahashi *et al.* 2005), the obtention of which sets the upper bound for the Ekman number range that we analyse in this study. The main equilibrium is therefore between the Coriolis torque Γ_C and the magnetic torque Γ_M, with a secondary contribution of the Reynolds stress torque Γ_R.

Our interpretation of the scaling law presented in Fig. 2 ties with the balance between Γ_C and Γ_M. We start with an evaluation of Γ_M. The classical theory of the omega effect (see for instance Moffatt 1978; Gubbins & Roberts 1987) states that a sphere in solid-body rotation with respect to a medium at rest, permeated by a poloidal magnetic field, undergoes a resistive magnetic torque of typical strength proportional to its rotation rate. Applying this principle to a set of concentric spheres with differences of solid-body rotation all bound by Ω_{ic} (Fig. 1d), permeated and rigidified by a poloidal field of typical amplitude B_r, a steady state balance between magnetic induction and magnetic dissipation will yield an induced azimuthal field bound by

$$B_\varphi = K\mu_0\sigma\Omega_{\mathrm{ic}} B_r D^2, \quad (5)$$

where μ_0 is the fluid magnetic permeability, and K is an interaction coefficient describing the relative geometry of the differential rotation and the poloidal magnetic field lines. The typical amplitude of the time-averaged magnetic torque thus writes

$$\Gamma_M = K\sigma\Omega_{\mathrm{ic}} B_r^2 D^5. \quad (6)$$

In Fig. 3, the radial profile of Γ_M is normalized by $\rho\Omega\Omega_{\mathrm{ic}} D^5$, in such a way that its value expresses the Elsasser number $\Lambda = K\sigma B_r^2/\rho\Omega$ of the interaction between poloidal magnetic field lines and differential rotation. We note that for the two cases that are shown, the normalized magnetic torque has about the same amplitude, confirming that the magnetic torque amplitude is indeed proportional to Ω_{ic}. Moreover, this also indicates that the Elsasser number of the interaction remains approximately constant: the system adjusts the geometry of the interaction in such a way to reduce K if B_r increases.

Our second step is to evaluate the Coriolis torque which balances the magnetic torque. The Coriolis torque can be expanded as

$$\Gamma_C = -2\rho\Omega \int_{V(r)} r \sin\theta \, \mathrm{u_s} \, \mathrm{d}V, \quad (7)$$

where $\mathrm{u_s}$ is the component of the velocity field along the cylindrical radial direction. Using $\nabla \cdot \mathbf{u} = 0$, one can substitute $r\sin\theta\,\mathrm{u_s} = \frac{1}{2}\nabla\cdot(s^2\mathbf{u})$ in (7) and by further using Gauss' theorem, the Coriolis torque can be written in terms of a surface integral

$$\Gamma_C = -\rho\Omega \int_{S(r)} r^2 \sin^2\theta \, \mathrm{u_r} \, \mathrm{d}S. \quad (8)$$

At a fluid-solid boundary, the no-penetration condition ensures that the Coriolis torque is zero. Within the fluid shell, the Coriolis torque does not vanish and is proportional to the amplitude u_r of the radial component of the flow. Our numerical dynamos, as well as similar configurations (Dormy *et al.* 1998; Sakuraba & Roberts 2009), contain three main sources for axisymmetric, long-term radial flow.

(i) Axial cell convection (Roberts 1965): This is the natural axisymmetric response to buoyancy gradients in a rapidly rotating fluid. It develops in an axial cell of thickness $E^{1/3}$ (Fig. 4a) and its contribution is negligible when multiplied by the term $\sin^2\theta$ present in the Coriolis torque integrand (see Fig. 4b).

(ii) Magnetostrophic winds (e.g. Sakuraba & Roberts 2009): These radial winds, locally driven by the Lorentz force through the balance which we are currently analysing, are mostly prominent close to the equatorial plane in our models [they are also present at the same location, but quite stronger in the simulations of Sakuraba & Roberts (2009), which use different temperature boundary conditions]. These winds are also responsible for driving super-rotation in a layer close to the equatorial plane in the simulations of Dormy *et al.* (1998). However, Dormy *et al.* (1998) note that their presence is a non-asymptotic effect, which tends to vanish as the Ekman number goes down to 0, provided the simulation Elsasser number stays of order 1.

(iii) Viscous (Ekman) circulation: This radial circulation is the strongest source in our models, mostly at the boundary of the tangent cylinder (see Fig. 4b). In the simulations of Dormy *et al.* (1998), viscous circulation is the only source of radial flow preventing the spherical surfaces from reaching complete solid-body rotation with the inner core (and the mantle) when the Ekman number tends towards 0.

From the previous discussion, we propose that the source of axisymmetric, long-term radial flow present in our models is representative

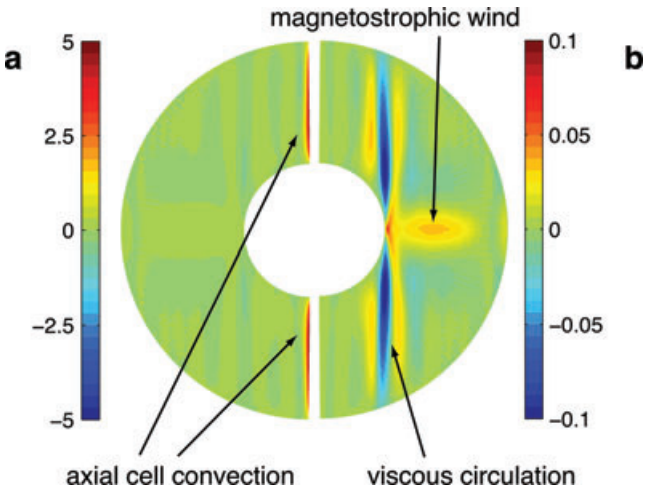

Figure 4. Meridional plane projection of the time and azimuthal average of (a) the radial velocity field $\mathrm{u_r}$, and (b) the Coriolis torque integrand $r^2\sin^2\theta\,\mathrm{u_r}$ (eq. 8), for the case presented in Fig. 1(b). Amplitudes are normalized with u_φ in (a) and $D^2 u_\varphi$ in (b).

Downloaded from http://gji.oxfordjournals.org/ at INIST-CNRS on April 27, 2016

of the asymptotic regime $E \to 0$ for a flow with global Elsasser number of order one (which is the case in our models, see last column of Table 1). Since the azimuthal average of u_r is dominated by Ekman pumping, it is then related to the amplitude of the zonal flow u_φ maintained by convection. It is important to emphasize that u_φ here includes all zonal flow components, not only those related to solid-body rotation differences within the fluid. Following classical Ekman pumping scaling, we can write

$$u_r \propto E^{1/2} u_\varphi. \tag{9}$$

An estimate of Γ_C is thus

$$\Gamma_C = K' \rho \Omega D^4 E^{1/2} u_\varphi, \tag{10}$$

where K' is a second geometrical constant. Equating our expressions Γ_M and Γ_C in (6) and (10) finally yields

$$\Omega_{\rm ic} D/u_\varphi = (K'/\Lambda) E^{1/2}. \tag{11}$$

Eq. (11) predicts that the ratio of the inner core rotation to outer core angular velocity scales as $E^{1/2}$, in good agreement with our numerical experiments shown in Fig. 2. Adjusting the scaling exponent on Fig. 2 to 1/2 requires a pre-factor $K'/\Lambda \approx 750$ or $K' \approx 7.5$ if $\Lambda \approx 10^{-2}$ (obtained from Fig. 3). The dependence on Λ in (11) is an illustration of Ferraro's law of corotation: the larger the radial magnetic field threading the geometry, the smaller is the allowed differential rotation between spherical surfaces.

3.2 Steady inner core rotation with gravitational coupling

In the previous section, we have seen that in the absence of gravitational coupling, it is impractical to determine the steady inner core rotation rate on the basis of the torque balance at the inner core boundary because corotation leads to vanishing time-averaged viscous and magnetic torques. The situation changes when a resistive gravitational torque exerted on the inner core is included in the simulation: the corotation within the viscous boundary layer is broken (Fig. 5a), and the inner core rotates at a rate $\Omega_{{\rm ic}/g}$ which is now smaller than the rotation rate Ω_f of the overlying fluid. This leads to a stronger viscous torque, and most importantly a much stronger (driving) magnetic torque, which can be approximated as (Dumberry 2007)

$$\Gamma_M(r_i) = \chi r_i^5 \sigma B_r({\rm ic})^2 (\Omega_f - \Omega_{{\rm ic}/g}), \tag{12}$$

where χ is a geometrical constant. This torque balances the time-averaged gravitational torque $\Gamma_G = -\Gamma\tau\Omega_{{\rm ic}/g}$ such that $\Gamma_M + \Gamma_G = 0$. Assuming that, in the presence of gravitational coupling, the overlying fluid continues to rotate at a rate Ω_f which is commensurate to the rate $\Omega_{\rm ic}$ of inner core rotation when gravitational coupling is absent, we obtain

$$\frac{\Omega_{{\rm ic}/g}}{\Omega_{\rm ic}} = \frac{1}{1+\alpha/\chi}, \tag{13}$$

where $\alpha = \Gamma\tau/r_i^5\sigma B_r({\rm ic})^2$ measures the relative amplitude of magnetic and gravitational torques at the inner boundary. This braking law is tested versus our numerical data (Fig. 5b), with good agreement (although our assumption that the overlying fluid remains unchanged is somewhat crude) if the geometrical constant is set to $\chi = 0.1$, independently of the Ekman number.

The convective dynamics in the fluid core is affected by inner core–mantle gravitational coupling through the restriction of the differential rotation between the inner core and the mantle. The amplitude of the zonal flows maintained by convection, including the differential rotation across the fluid core, must then comply with this restriction. The steady inner core rotation $\Omega_{{\rm ic}/g}$ in presence of gravitational coupling is thus never as fast as the rate $\Omega_{\rm ic}$ reached in the corresponding situation without gravitational coupling, and follows the same Ekman-number dependency as in simulations with no gravitational coupling. The upper bound on $\Omega_{\rm ic}$ can then be determined by the scaling expressed in eq. (11).

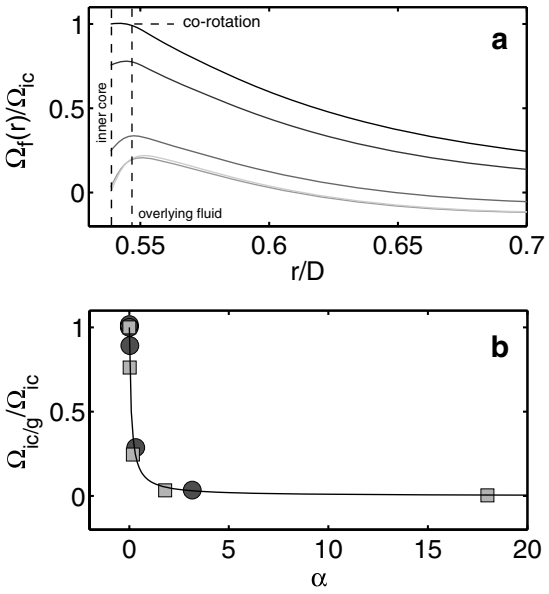

Figure 5. (a) Radial profile of the time-averaged solid body rotation rate $\Omega_f(r)$ (as defined in Fig. 1d), normalized by the inner core rotation rate $\Omega_{\rm ic}$ without gravitational coupling. Shown are the cases represented in Fig. 1(a) where $\Gamma\tau = 0$ (black line) and cases with the same parameters but $\Gamma\tau = 50, 500, 5000, 50\,000$ (lines of increasingly light grey colour). The vertical dashed lines approximately represent the thickness $\sqrt{E}$ of the Ekman viscous layer in that case. (b) Ratio $\Omega_{{\rm ic}/g}/\Omega_{\rm ic}$ of steady inner core rotation with respect to the inner core rotation rate without gravitational coupling, as a function of $\alpha = \Gamma\tau/r_i^5\sigma B_r({\rm ic})^2$, in two cases where gravitational coupling is gradually increased from the reference situations of Figs 1(a) ($E = 3 \cdot 10^{-5}$, squares) and 1(c) ($E = 3 \cdot 10^{-6}$, circles). The solid line is a prediction of a model where $\Omega_{{\rm ic}/g}/\Omega_{\rm ic} = 1/(1+\alpha/\chi)$, where χ is set to 0.1 for both series of models.

3.3 Long-term fluctuations of inner core rotation

Owing to the large viscosity employed in our simulations, the system does not produce fluctuations on timescales much shorter than the overturn time (see Fig. 6), unlike in the Earth's core as is evident from the observed rapid secular variation (Olsen & Mandea 2008; Gillet *et al.* 2010). Our models only capture the long-term fluctuations, on timescales equal to or longer than the overturn time. The amplitude of fluctuations in our system can therefore be seen as a lower bound for the Earth's core, over which additional short-term fluctuations should be superimposed.

Long-term inner core rotation fluctuations are not expected to follow the scaling law (11) because the inner core inertia enters the balance and can accommodate large variations of the magnetic torque at the inner boundary. Fig. 6 shows that as the Ekman number is decreased, the inner core rotation fluctuations become comparatively larger with respect to the steady component of rotation. Since these fluctuations arise due to fluctuations in the magnetic and viscous torques at the inner core boundary (see eq. 1), corresponding

Downloaded from http://gji.oxfordjournals.org/ at INIST-CNRS on April 27, 2016

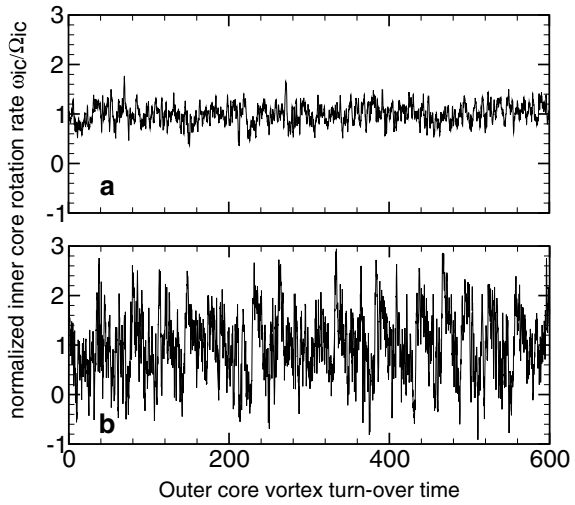

Figure 6. Time-series of the instantaneous inner core rotation rate $\omega_{\rm ic}$, normalized by its time-averaged value $\Omega_{\rm ic}$, for the runs presented in Fig. 1(a) (panel a) and 1(c) (panel b), which respectively have $E = 3 \cdot 10^{-5}$ and $E = 3 \cdot 10^{-6}$. Time is normalized by the outer core overturn time D/U, where U is the root-mean-squared, time-averaged velocity in the fluid outer core.

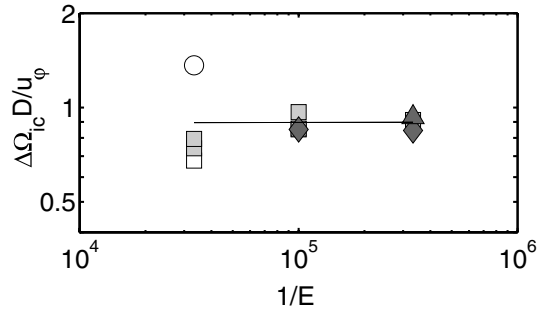

Figure 7. Ratio $\Delta\Omega_{\rm ic} D/u_\varphi$ of the standard deviation of inner core rotation fluctuations to fluid outer core angular velocity, as a function of the inverse Ekman number $1/E$. Symbol colours and shapes as in Fig. 2. The solid line is the result of a least-squares logarithmic fit yielding $\Delta\Omega_{\rm ic} D/u_\varphi = 0.9E^{0.0}$. The 2σ uncertainty range on exponent is ± 0.1.

to variations of the outer core zonal flow and magnetic field over advective timescales, it is natural to expect a Strouhal number of order 1 behaviour, that is, that they will remain commensurate with the outer core angular velocity u_φ/D, that is,

$$\Delta\Omega_{\rm ic} D/u_\varphi \approx 1. \qquad (14)$$

This relationship reveals good agreement with numerical data in Fig. 7.

4 DISCUSSION

Our study reveals that the solid-body rotation of spherical surfaces in the fluid outer core (the part of the thermal wind flow which drives inner core rotation) is limited by a torque balance between Lorentz and Coriolis forces. In our simulations, the resistive magnetic torque results from an inductive omega effect created by the differential rotation acting on the poloidal magnetic field. This torque is balanced by a torque from the Coriolis force acting on the radial flow generated by Ekman pumping, which, as we argued, is the only source of axisymmetric, long-term radial circulation asymptotically preventing the spherical fluid surfaces from reaching complete solid-body rotation with the inner core and the mantle.

In the absence of gravitational coupling the inner core must be corotating with the fluid near the inner core boundary. Therefore, the rate of differential rotation of the inner core with respect to the mantle must be equal to the dynamically maintained differential rotation across the fluid shell. The torque balance that describes this differential rotation leads to a ratio $\Omega_{\rm ic} D/u_\varphi$ between the rate of inner core rotation and typical angular velocities within the fluid core which decreases as the square root of the Ekman number. The inclusion of gravitational coupling between the inner core and mantle does not alter this scaling, though it acts to further reduce the rate of inner core rotation.

The range over which we observe this decrease is admittedly small when compared to the distance between our models and the Earth's core value $E \approx 3 \cdot 10^{-15}$, obtained with $\nu = 1.2 \cdot 10^{-6}\,{\rm m^2\,s^{-1}}$ (de Wijs *et al.* 1998), $\Omega = 7.29 \cdot 10^{-5}\,{\rm 1\,s^{-1}}$ and $D = 2200\,{\rm km}$. In our set of numerical models, the practical upper bound on E is set by the requirement that viscous torques should be much smaller than magnetic torques, while the lower bound is set by the current limits of accessible computer power. If the torque balance which we observe in the numerical models pertains to the Earth's dynamo conditions, at $E = 3 \cdot 10^{-15}$ we expect $\Omega_{\rm ic} D/u_\varphi$ to be no greater than $(K'/\Lambda)E^{1/2} = O(10^{-5})$ where we have used $K'/\Lambda = 750$. As the outer core flow angular velocity amounts to $u_\varphi/D \approx 0.1^{\rm o}\,{\rm yr^{-1}}$ (Hulot *et al.* 2002; Amit & Olson 2006), we expect the steady differential rotation of the inner core not to exceed a value of a few degrees per million years.

Obviously, it is possible that the torque balance observed in our models does not apply to the Earth's core conditions, for instance if the torque from Reynolds stresses becomes larger than the Coriolis torque and provides the main balance to the magnetic torque. Indeed, an equilibrium between the Coriolis and inertial torques is established in non-magnetic convection, yielding a zonal flow morphology dominated by an axially rigid component. A proportionally larger contribution of the torque from Reynolds stresses can thus allow a larger inner core rotation rate. However, in numerical configurations similar to the ones we presented here, large inertial forces result in a dynamo which loses its dominant dipole (Aubert 2005; Christensen & Aubert 2006). In a dipole-dominated regime, an inertial-magnetic torque balance is not observed, and therefore we lack the numerical models appropriate for exploring this situation.

Our proposed steady inner core rotation rate is much smaller than the seismically inferred rates of inner core rotation at a few tenths of degrees per year. Therefore, the seismic observations cannot represent a steady rotation. However, these rates are perfectly in line with the amplitude $\Delta\Omega_{\rm ic} \approx u_\varphi/D$ of long-term inner core rotation fluctuations. We thus propose that the present-day inner core rotation is a fragment of a time-varying signal, rather than a steady super-rotation.

Geodetic data provide another handle on the Earth's inner core rotation fluctuations. By virtue of gravitational coupling, these should indeed entrain fluctuations in mantle rotation. Since the latter cannot exceed the observed decadal variations in the length-of-day (Buffett & Creager 1999; Dumberry 2007), this allows to place bounds on the strength of gravitational coupling such that it is compatible with an inner core with fluctuating rotation. Assuming an inner core oscillating with an amplitude of $0.3^{\rm o}\,{\rm yr^{-1}}$ at a period longer than 60 yr [a reasonable lower bound since the seismic data span about 30 yr with some evidence (Song & Poupinet 2007) of non-stationarity over that period], and electromagnetic coupling of

Downloaded from http://gji.oxfordjournals.org/ at INIST-CNRS on April 27, 2016

reasonable strength at the core–mantle boundary, this constraint places an upper bound $\Gamma\tau \leq 5 \cdot 10^{19}$ N m yr on the strength of the gravitational coupling (Dumberry & Mound 2010). This value is more than one order of magnitude smaller than a previous estimate. Numerical values $\Gamma = 3 \cdot 10^{20}$ N m and $\tau \geq 6$ yr have been suggested by interpreting a 6-yr oscillation in the length-of-day (Abarca del Rio *et al.* 2000) as the period of the free mode of mantle-inner core gravitational (MICG) coupling (Mound & Buffett 2006), the value of Γ being also compatible with early models of the long-wavelength geoid at the core–mantle boundary (CMB) (Forte & Peltier 1991; Defraigne *et al.* 1996) with peak-to-peak variations of approximately 300 m. Lowering Γ or τ implies that either the period, or the amplitude of the MICG mode can no longer account for the 6-yr length-of day signal, and an alternative explanation is required. Fast torsional oscillations in the fluid core (Alfvén waves involving geostrophic flows) supported by a radial magnetic field of 2–3 mT can explain the 6-yr signal (Gillet *et al.* 2010). Such a field strength is larger than earlier estimates (Zatman & Bloxham 1997) based on slower torsional oscillations but is in better agreement with recent predictions of the magnetic field amplitude inside the core (Christensen & Aubert 2006; Aubert *et al.* 2009). Our results thus provide additional support for this scenario. Releasing the MICG constraint on Γ is also in line with more recent models of the geoid at the CMB (Simmons *et al.* 2006) which favour smaller peak-to-peak variations, and suggest Γ in the range of $2 - 3 \cdot 10^{19}$ N m. It should finally be noted that within the framework of our model, the value $\Gamma\tau \leq 5 \cdot 10^{19}$ N.m.yr together with $\sigma = 5 \cdot 10^5$ S m^{-1}, $B_r = 2$ mT and $r_i = 1200$ km (Dumberry 2007) yields a weak amount $\alpha/\chi \leq 0.3$ per cent of long-term inner core gravitational braking.

A further consequence of our results concerns the westward drift of magnetic field features observed in the secular variation. Our analysis suggests that the steady solid-body rotation of the fluid below the core–mantle boundary should remain below a few degrees per million years everywhere in the fluid. This implies that if the westward drift, with a typical rate of 0.2° yr^{-1} (e.g. Finlay & Jackson 2003), is caused by an underlying steady westward flow, there must be equal amounts of steady eastward flow when integrating over a spherical surface below the core–mantle boundary (though this flow may not be seen if it is predominantly located in areas where there are no magnetic field features to be advected). Alternatively, it could imply that a large part of the westward drift represents the phase velocity of an MHD wave propagating westwards rather than a mean steady flow. If the recent secular variation does contain a solid-body westward rotation (e.g. Amit & Olson 2006), then our results imply that this rotation is not steady but must instead be fluctuating on long timescales, as is partially supported by archaeomagnetic secular variation (Dumberry & Finlay 2007).

Our final remark is that the maximal steady inner core rotation rate which we predict is marginally too high to warrant texturing mechanisms of the inner core surface by mantle-induced thermochemical winds on a timescale of 100 Myr (Aubert *et al.* 2008). On this timescale, the inner core could indeed drift out of alignment with the mantle but would not perform a large number of revolutions, thus preserving the possibility of a longitudinally asymmetric signature from the mantle. It is also possible that a gravitational torque driven by the aspherical inner core growth induces an inner core rotation at similar rates but in the reverse direction (Dumberry 2010) and thereby slow down the overall rate of inner core rotation. Better seismic constraints on the time variations in inner core rotation, combined with further investigation of the long-term nature of outer core flows, are needed to better understand the nature of the coupling between the mantle, the outer core and the inner core.

ACKNOWLEDGMENTS

We wish to thank two anonymous referees for helpful and constructive reviews, and D. Jault and G. Hulot for discussions. This work was supported by program SEDIT of French Institut National des Sciences de l'Univers and CNRS. MD is supported by a Discovery grant from NSERC/CRSNG. Numerical computations were performed at S-CAPAD, IPGP, France and at HPC resources from GENCI-CINES and GENCI-IDRIS (Grant 2009-042122 and 2010-042122). This is IPGP contribution 3068.

REFERENCES

Abarca del Rio, R., Gambis, D. & Salstein, D., 2000. Interannual signals in length of day and atmospheric angular momentum, *Ann. Geophys.,* **18,** 347–364.

Amit, H. & Olson, P., 2006. Time average and time dependent parts of core flow, *Phys. Earth planet. Int.,* **155,** 120–139, doi: 10.1016/J.pepi.2005.10.006.

Aubert, J., 2005. Steady zonal flows in spherical shell dynamos, *J. Fluid. Mech.,* **542,** 53–67.

Aubert, J., Amit, H. & Hulot, G., 2007. Detecting thermal boundary control in surface flows from numerical dynamos, *Phys. Earth planet. Int.,* **160,** 143–156.

Aubert, J., Amit, H., Hulot, G. & Olson, P., 2008. Thermochemical flows couple the Earth's inner core growth to mantle heterogeneity, *Nature,* **454**(7205), 758–761.

Aubert, J., Aurnou, J. & Wicht, J., 2008. The magnetic structure of convection-driven numerical dynamos, *Geophys. J. Int.,* **172,** 945–956.

Aubert, J., Labrosse, S. & Poitou, C., 2009. Modelling the palæo-evolution of the geodynamo, *Geophys. J. Int.,* **179,** 1414–1428.

Aurnou, J. & Olson, P., 2000. Control of inner core rotation by electromagnetic, gravitational and mechanical torques, *Phys. Earth planet. Int.,* **117**(1-4), 111–121.

Aurnou, J.M., Brito, D. & Olson, P.L., 1996. Mechanics of inner core superrotation, *Geophys. Res. Lett.,* **23**(23), 3401–3404.

Aurnou, J., Brito, D. & Olson, P., 1998. Anomalous rotation of the inner core and the toroidal magnetic field, *J. geophys. Res.,* **103**(B5), 9721–9738.

Buffett, B., 1996. Gravitational oscillations in the length of day, *Geophys. Res. Lett.,* **23**(17), 2279–2282.

Buffett, B., 1997. Geodynamic estimates of the viscosity of the Earth's inner core, *Nature,* **388**(6642), 571–573.

Buffett, B. & Creager, K., 1999. A comparison of geodetic and seismic estimates of inner-core rotation, *Geophys. Res. Lett.,* **26**(10), 1509–1512.

Buffett, B.A. & Glatzmaier, G.A., 2000. Gravitational braking of inner-core rotation in geodynamo simulations, *Geophys. Res. Lett.,* **27**(19), 3125–3128.

Cao, A., Masson, Y. & Romanowicz, B., 2007. Short wavelength topography on the inner-core boundary, *PNAS,* **104**(1), 31–35.

Christensen, U. & Aubert, J., 2006. Scaling properties of convection-driven dynamos in rotating spherical shells and application to planetary magnetic fields, *Geophys. J. Int.,* **117,** 97–114.

Christensen, U.R. *et al*., 2001. A numerical dynamo benchmark, *Phys. Earth planet. Int.,* **128,** 25–34.

Defraigne, P., Dehant, V. & Wahr, J.M., 1996. Internal loading of an inhomogeneous compressible Earth with phase boundaries, *Geoph. J. Int.,* **125,** 173–192.

Dormy, E., Cardin, P. & Jault, D., 1998. MHD flow in a slightly differentially rotating spherical shell, with conducting inner core, in a dipolar magnetic field, *Earth. planet. Sci. Lett.,* **160**(1–2), 15–30.

Downloaded from http://gji.oxfordjournals.org/ at INIST-CNRS on April 27, 2016

Dumberry, M., 2007. Geodynamic constraints on the steady and time-dependent inner core axial rotation, *Geophys. J. Int.,* **170**(2), 886–895.
Dumberry, M., 2010. Gravitationally driven inner core differential rotation, *Earth planet. Sci. Lett.,* **297,** 387–394.
Dumberry, M. & Finlay, C., 2007. Eastward and westward drift of the Earth's magnetic field for the last three millennia, *Earth planet. Sci. Lett.,* **254,** 146–157.
Dumberry, M. & Mound, J., 2010. Inner core-mantle gravitational locking and the super-rotation of the inner core, *Geophys. J. Int.,* **181**(2), 806–817.
Ferraro, V.C.A., 1937. The non-uniform rotation of the sun and its magnetic field, *Mon. Not. R. astr. Soc.,* **97,** 458–472.
Finlay, C. & Jackson, A., 2003. Equatorially dominated magnetic field change at the surface of Earth's core, *Science,* **300,** 2084–2086.
Forte, A.M. & Peltier, R., 1991. Viscous flow models of global geophysical observables 1. forward problems, *J. geophys. Res.,* **96**(B12), 20 131–20 159.
Gillet, N., Jault, D., Canet, E. & Fournier, A., 2010. Fast torsional waves and strong magnetic field within the Earth's core, *Nature,* **465,** 74–77.
Glatzmaier, G.A. & Roberts, P.H., 1996. Rotation and magnetism of Earth's inner core, *Science,* **274**(5294), 1887–1891.
Gubbins, D., 1981. Rotation of the inner core, *J. geophys. Res.,* **86**(NB12), 1695–1699.
Gubbins, D. & Roberts, P.H., 1987. Magnetohydrodynamics of the Earth's core, in *Geomagnetism,* Vol. 2, ed. Jacobs, J.A., Academic Press, London.
Hollerbach, R., 1998. What can the observed rotation of the Earth's inner core reveal about the state of the outer core? *Geophys. J. Int.,* **135**(2), 564–572.
Hulot, G., Eymin, C., Langlais, B., Mandea, M. & Olsen, N., 2002. Small-scale structure of the geodynamo inferred from Oersted and Magsat satellite data, *Nature,* **416,** 620–623.
Laske, G. & Masters, G., 2003. The Earth's free oscillations and differential rotation of the inner core, in *Earth's Core: Dynamics, Structure, Rotation,* Vol. 31, eds Dehant, V., Creager, K., Zatman, S. & Karato, S., AGU monograph, Washington, DC.
Moffatt, K., 1978. *Magnetic field generation in electrically conducting fluids,* Cambridge University Press.
Mound, J.E. & Buffett, B.A., 2006. Detection of a gravitational oscillation in length-of-day, *Earth planet. Sci. Lett.,* **243**(3–4), 383–389.
Olsen, N. & Mandea, M., 2008. Rapidly changing flows in the Earth's core, *Nature Geosci.,* **1**(6), 390–394.
Roberts, P.H., 1965. On the thermal instability of a highly rotating fluid sphere, *Astr. J.,* **141,** 240–250.
Sakuraba, A. & Roberts, P.H., 2009. Generation of a strong magnetic field using uniform heat flux at the surface of the core, *Nature Geosci.,* **2**(11), 802–805.
Simmons, N.A., Forte, A.M. & Grand, S.P., 2006. Constraining mantle flow with seismic and geodynamic data: a joint approach, *Earth planet. Sci. Lett.,* **246,** 109–124.
Song, X. & Richards, P., 1996. Seismological evidence for differential rotation of the Earth's inner core, *Nature,* **382**(6588), 221–224.
Song, X.D. & Poupinet, G., 2007. Inner core rotation from event-pair analysis, *Earth planet. Sci. Lett.,* **261**(1–2), 259–266.
Souriau, A., 2007. The Earth's cores, in *Treatise on Geophysics. 1- Seismology and Structure of the Earth,* Vol. 11, pp. 655–693, eds Dziewonski, A. & Romanowicz, B., Elsevier, Amsterdam.
Takahashi, F., Matsushima, M. & Honkura, Y., 2005. Simulations of a quasi-taylor state geomagnetic field including polarity reversals on the earth simulator, *Science,* **309**(5733), 459–461.
Wen, L.X., 2006. Localized temporal change of the Earth's inner core boundary, *Science,* **314**(5801), 967–970.
de Wijs, G., Kresse, G., Vocadlo, L., Dobson, D., Alfe, D., Gillan, M. & Price, G., 1998. The viscosity of liquid iron at the physical conditions of the Earth's core, *Nature,* **392**(6678), 805–807.
Zatman, S. & Bloxham, J., 1997. Torsional oscillations and the magnetic field within the Earth's core, *Nature,* **388,** 760–763.

Downloaded from http://gji.oxfordjournals.org/ at INIST-CNRS on April 27, 2016